

# A simple approach for experimental characterization and validation of proton pencil beam profiles

Paulina Stasica<sup>1,2</sup>, Jakub Baran<sup>1</sup>, Carlos Granja<sup>3</sup>, Nils Krah<sup>4</sup>, Grzegorz Korcyl<sup>5</sup>, Cristina Oancea<sup>3</sup>, Monika Pawlik-Niedźwiecka<sup>1,5</sup>, Szymon Niedźwiecki<sup>5</sup>, Marzena Rydygier<sup>1</sup>, Angelo Schavi<sup>6</sup>, Antoni Rucinski<sup>1</sup>, Jan Gajewski<sup>1\*</sup>

<sup>1</sup>*Institute of Nuclear Physics PAN, Krakow, Poland*

<sup>2</sup>*AGH University of Science and Technology, Krakow, Poland*

<sup>3</sup>*ADVACAM, Prague, Czech Republic*

<sup>4</sup>*CNRS/CREATIS, UMR 5220, Lyon, France*

<sup>5</sup>*Institute of Physics, Jagiellonian University, Krakow, Poland*

<sup>6</sup>*Sapienza University of Rome, Italy*

Correspondence\*:

Jan Gajewski

jan.gajewski@ifj.edu.pl

## 2 ABSTRACT

3 A precise characterization of therapeutic proton pencil beams is essential for commissioning of  
4 any treatment planning system (TPS). The dose profile characterization includes measurement  
5 of the beam lateral dose profile in the beam core and far from the beam core, in the so called  
6 low-dose envelope, and requires a sophisticated detection system with a few orders of magnitude  
7 dynamic range. We propose to use a single-quantum sensitive MINIPix TIMEPIX detector,  
8 along with an in-house designed holder to perform measurements of the pencil beam dose  
9 profile in air and in water. We validated the manufacturer calibration of the MINIPix TIMEPIX  
10 detector in proton beams of various energies and compared the deposited energy spectra to  
11 Monte Carlo (MC) simulations. The precision of the lateral dose profile measurements has  
12 been systematically validated against Krakow proton facility commissioning data and dose  
13 profile simulations performed with MC codes GATE/Geant4 and FRED. We obtained an excellent  
14 agreement between MINIPix TIMEPIX measurements and simulations demonstrating the feasibility  
15 of the system for a simple characterization and validation of proton pencil beams. The proposed  
16 approach can be implemented at any proton therapy facility to acquire experimental data needed  
17 to commission and validate analytical and MC based TPS.

18 **Keywords:** Proton therapy; Dose; Semiconductor pixel detector; Timepix detector; Monte Carlo simulation

## 1 INTRODUCTION

19 The dosimetric advantage of proton beams in radiotherapy is due to their depth-dose distribution (Bragg  
20 curve), which enable to minimize dose deposited in healthy tissues and to maximize it in the tumor region  
21 [1, 2]. After many years of research and development, a growing interest in proton radiotherapy is observed.

22 According to data provided by the Particle Therapy Co-Operative Group (<https://www.ptcog.ch/>,  
23 2020) there are 91 proton (or proton and carbon ion) radiotherapy facilities in operation, 33 under  
24 construction, and 27 in the planning stage, all around the world. At the start-up of each new proton facility,  
25 for the purpose of launching a treatment planning system (TPS), a commissioning of the proton pencil  
26 beam is required. The beam commissioning that includes, i.a., an experimental characterization of lateral  
27 and longitudinal beam profiles, is a demanding and time-consuming experimental procedure. In this paper  
28 we propose a new approach for characterization of lateral beam profiles in air and in water to simplify the  
29 procedure of commissioning of TPS and its validation.

30 The state-of-the-art experimental approach for proton beam commissioning is to measure lateral dose  
31 profiles in air with a scintillating screen [3]. This method allows only to measure the major component  
32 of the lateral beam dose profile characterized by a Gaussian distribution. In fact, primary particles scatter  
33 on the passive components of a beam delivery system, such as gantry nozzle equipment and range  
34 shifters/compensators, building up an additional dose envelope of the lateral beam profiles [3], which is  
35 recognized as a nuclear halo. The nuclear halo is often approximated in TPS by double Gaussian model  
36 of proton pencil beam. The accurate characterization of pencil beam lateral dose profiles is particularly  
37 important for facilities using very small spot sizes as the uncertainty of the nuclear halo modeling is  
38 propagated over a greater number of spots [3, 4]. Also, the effect is pronounced for small, shallowly located  
39 targets that are irradiated with a limited number of spots because the uncertainties are not averaged [4].  
40 Still, the measurements of the dose envelope are often neglected, because characterization of pencil beam  
41 nuclear halo requires dedicated detector technology with sufficient sensitivity and accuracy.

42 In order to compensate for the uncertainties in the beam modeling caused by the dose envelope some of  
43 the proton centers investigate and develop new detection techniques for characterization of the lateral beam  
44 profile far from the beam core. For instance, in Krakow proton facility, passive dosimetry [5, 6] or single  
45 particle sensitive methods like scCVD diamond detectors [7] have been investigated. Refer to a review of  
46 Karger et al. and references for description of other approaches [8].

47 After commissioning stage, a validation of the beam model implementation in TPS is required, and it  
48 is typically performed by means of experimental measurements in water. Usually, the dose in complex  
49 radiation fields consisting of several pencil beams is measured and, if necessary, field size factors are  
50 applied to correct for experimental and computational uncertainties of the pencil beam modeling. The  
51 introduction of Monte Carlo (MC) tools in the clinical routine offers computational accuracy allowing  
52 consideration of nuclear halo in patient treatment plan simulations. However, the experimental validation  
53 of single pencil beam dose profiles in water, including the nuclear halo, is even more demanding than in  
54 air, because requires operation of the detector in water. There is still a necessity to provide more accurate,  
55 fast, and easy-to-use experimental methods for characterization of the low-dose envelope of proton pencil  
56 beams.

57 Here, we propose a simple approach for experimental characterization and validation of lateral and  
58 longitudinal dose profiles including the dose envelope. We used a commercial semiconductor pixel detector,  
59 MINIPIX TIMEPIX, for fast and high-precision particle-by-particle measurements of a therapeutic proton  
60 beam. We present an experimental setup consisting of the MINIPIX TIMEPIX detector, in-house developed  
61 detector holder, and water phantom, that can be used for both, commissioning measurements in air and  
62 validation measurements in water. We measured pencil beam profiles and compared the results to the  
63 facility commissioning data, TPS calculations, and Monte Carlo (MC) simulations, demonstrating the  
64 feasibility of the approach.

## 2 MATERIALS AND METHODS

### 65 2.1 Proton radiotherapy facility

66 The Krakow proton beam facility is in clinical operation since October 2016, offering protons for radiation  
67 therapy treatment, as well as for physics and radiobiology experiments. The Krakow facility offers stable  
68 beam intensities ranging from 1 to 300 nA and scanning pencil beam in energy range from 70 to 226 MeV,  
69 which corresponds to range in water from 4.2 cm to 31.8 cm. The lateral beam size ( $1\sigma$ ) ranges depending  
70 on the proton beam energy and application of a range modulator (range shifter - RS) from about 3 to 15 mm.  
71 The RS made of 4.2 cm thick PMMA material, mounted at the gantry nozzle is used to modulate proton  
72 range.

73 In Krakow, Eclipse TPS from Varian (version 13.6), commissioned against experimental data, is used for  
74 treatment planing. Longitudinal dose profile measurements were performed in water using a Bragg Peak  
75 Chamber (from PTW). Lateral dose profiles in air were measured using LYNX scintillating screen (IBA  
76 Dosimetry) and thermoluminescence detectors (TLDs) in the primary Gaussian and the dose envelope  
77 regions, respectively. Eclipse TPS was used to compute 3D pencil beam dose profiles in water. In addition  
78 to clinical TPS, the dose profiles were simulated using a secondary dose computation tool, FRED MC code  
79 [9] that was commissioned and validated for quality assurance purposes in Krakow [10]. The proton beam  
80 model used by clinical TPS and FRED have been adopted for GATE/Geant4 simulations performed in this  
81 work.

### 82 2.2 MINIPIX TIMEPIX Detector and data acquisition software

83 In this study we propose using the technology of pixel semiconductor detectors, TIMEPIX from  
84 ADVACAM (<https://advacam.com>), for characterization of therapeutic proton pencil beams and  
85 validation of TPS and MC simulations. Due to the single-quantum sensitivity and particle tracking  
86 capability, TIMEPIX technology enables particle-by-particle dosimetry of proton pencil beams. TIMEPIX is  
87 a commercial version of MEDIPIX detector developed at CERN and is widely used for radiation research,  
88 e.g., in ion beam therapy [11, 12], in radiation dosimetry [13, 14, 15], in particle accelerator environments  
89 [16] or for space radiation characterization on board of the International Space Station [17, 18, 19].

90 In this work a compact MINIPIX TIMEPIX detector was used (figure 1, left). The entire MINIPIX  
91 TIMEPIX has dimensions of  $77 \times 21 \times 10$  mm and its total weight is 25 g. The sensitive volume of the  
92 semiconductor silicon sensor ( $14.08 \times 14.08 \times 0.3$  mm) consists of a 2D array of  $256 \times 256$  pixels, each has  
93 dimensions of  $55 \times 55 \mu\text{m}$ . The ionizing particle penetrating the sensitive volume of the MINIPIX TIMEPIX  
94 produces electric charge, which is collected by adjacent electrode pixels forming a cluster. The signal  
95 read-out is performed in each pixel individually in single frame acquisition time of typical length of about  
96 1-100 ms. The MINIPIX TIMEPIX frame readout dead-time is 22 ms. Data acquisition electronics is fully  
97 integrated, connected to the computer via USB port and does not require a dedicated cooling system. For  
98 more details on the TIMEPIX detector technology refer to [20, 21, 22] and references.

99 The MINIPIX TIMEPIX detector is equipped with a data acquisition and real-time visualization software,  
100 PIXET PRO, which also provides data processing tools for cluster morphology analysis. Figure 1 (right)  
101 shows an example of data frame acquired in Krakow. The morphology of each cluster, consisting of the  
102 signal amplitude in a number of adjacent pixels, is characterized by a list of cluster parameters, including:  
103 the position of the cluster center of mass, the total energy deposited, the cluster length, and the angle at  
104 which the particle enters the detector. The cluster analysis enable identification of impinging particle type  
105 [21]. The analysis of multiple clusters enables particle-by-particle experimental characterization of the  
106 mixed radiation fields consisting of primary and secondary protons, secondary electrons, photons, etc.  
107 Depending on the primary particle fluence, the single frame acquisition time need to be adjusted for each

108 measurement individually, in order to minimize the overlapping of the clusters. The cluster overlapping  
109 effect occurs when different particles at short time intervals produce clusters which are so close to each  
110 other that they overlap and are recognized by PIXET PRO software as a single cluster of larger energy  
111 deposition. The overlapping effect does not influence the total energy deposited in the detector.

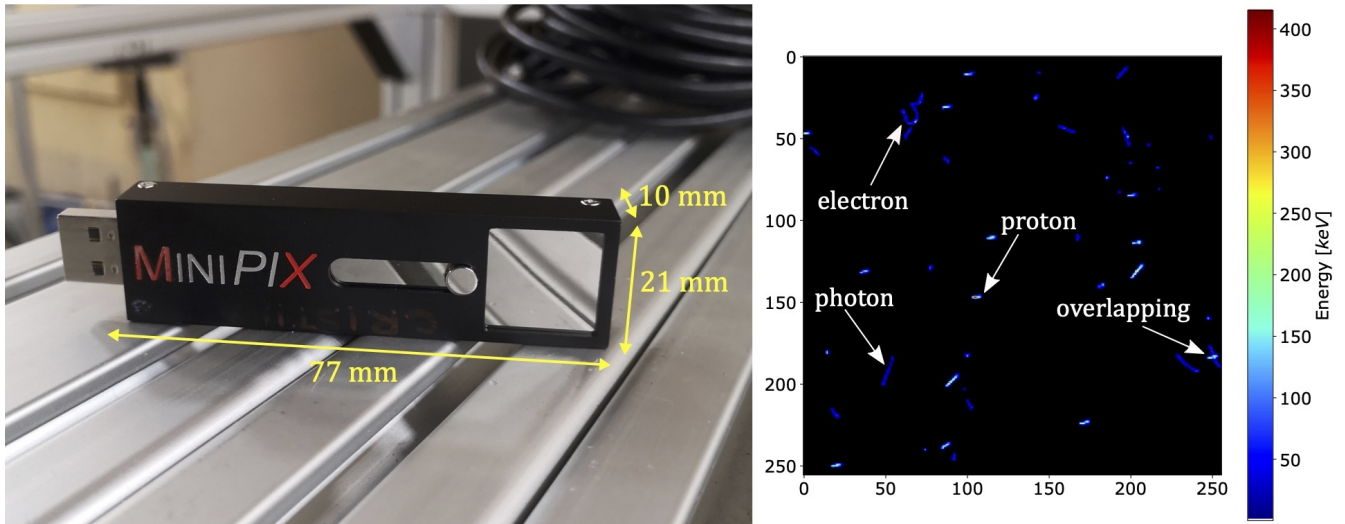


**Figure 1.** The MINIPIX TIMEPIX detector equipped with a ASIC and 300  $\mu\text{m}$  thick silicon sensor (left) and an example frame obtained from the measurements (right). Clusters are produced by different particles in mixed radiation field of proton pencil beam in water. Low-LET, narrow, curly tracks are typical for electrons, high-LET, wide, straight tracks for energetic heavy charged particles such as protons, while low-LET, straight tracks are characteristic for photons. In the right side of the frame an example of overlapping clusters is shown.

## 112 2.3 Dose calculation engines

113 In this work, the dose distributions were calculated using clinical TPS Eclipse, as well as two MC toolkits:  
114 GATE/Geant4 (version 8.2), interfaced to Geant4 (version 10.4.p2) [23] and FRED MC (version 3.0.18)  
115 [9]. GATE/Geant4 is a full MC simulation engine transporting all the primary and secondary particles  
116 contributing to the dose deposition. FRED is a fast, GPU-accelerated MC tool transporting primary and  
117 secondary protons, deuterons, and tritons, whereas the energy from gammas and delta-electrons is deposited  
118 at their production point.

## 119 2.4 Calibration measurements

120 The MINIPIX TIMEPIX detector is calibrated by the manufacturer aiming at a uniform response of  
121 each individual pixel to energy depositions from X-rays source [22, 24, 25]. In principal, primary and/or  
122 secondary particles can enter the detector surface at any angle, which specially occurs measuring mixed  
123 radiation field produced by a proton beam in water. In this work, we performed a validation of the detector  
124 response to proton beams impinging the detector surface at different angles by comparing the energy  
125 deposition spectra obtained experimentally to MC simulations.

### 126 Experimental setup and data acquisition

127 The MINIPIX TIMEPIX was exposed to proton pencil beams of nominal energies E70, E100, E150,  
128 and E200, corresponding to proton mean energies and energy spreads (standard deviation) at the detector  
129 position of 70.5(0.6) MeV, 100.1(0.8) MeV, 149.9(1) MeV, and 199.6(1) MeV, respectively. For each  
130 nominal energy the detector was positioned at the isocentre in air (in the beam core) at  $\beta$  angles ranging  
131 from 27° to 83°. We defined  $\beta$  as the angle between the normal to the silicon sensor surface and the proton  
132 beam axis (cf. figure 2). The accelerator dark current was used allowing to keep the particle fluence low  
133 enough to avoid saturation of the detector and to minimize the cluster overlapping.

### 134 Monte Carlo simulations

135 We performed MC simulations of the calibration setup in GATE/Geant4 toolkit. The MINIPIX  
136 TIMEPIX detector active volume was simulated as a  $14.08 \times 14.08 \times 0.3$  mm<sup>3</sup> cube made out of silicon  
137 ( $\rho = 2.33$  g/cm<sup>3</sup>,  $I_{\text{pot}} = 173$  eV [26]). The detector was positioned at the isocentre at  $\beta$  angles mimicking  
138 the experimental conditions. For simulations of proton pencil beams, the MC implementation of the  
139 clinical beam model based on Krakow proton facility commissioning measurements was used. We used the  
140 QGSP\_BIC\_HP\_EMZ physics list with production cuts in the active volume of 10  $\mu$ m for protons, electrons,  
141 and gammas. For each individual calibration simulation the total number of 10<sup>6</sup> primary particles were  
142 simulated. Using a phase space actor in GATE/Geant4 we scored the type, energy, angle, and position of  
143 the incidence of each primary particle crossing the detector surface. The history of the interactions and  
144 energy depositions of primary and secondary particles of unique identification number (UID) was scored  
145 using a GATE/Geant4 sensitive volume.

### 146 Data analysis

147 The results scored by the phase space actor and the GATE/Geant4 sensitive volume were merged based  
148 on the primary particle UID. The total energy deposited in the detector by a single primary proton was  
149 calculated as a sum of all energy depositions from the primary and secondary particles scored inside the  
150 GATE/Geant4 sensitive volume.

151 For each primary proton energy and detector angular position ( $\beta$ ), the energy deposition distributions  
152 obtained from the MINIPIX TIMEPIX measurements were compared to the GATE/Geant4 simulations.  
153 In order to account for differences in experimental and MC simulation setups, we applied filtering of

154 experimental data. The list of clusters obtained with MINIPix TIMEPIX was filtered for the measured  
155 angle at which the particle entered the detector with the condition  $\beta \pm 3^\circ$ . In addition we compared the  
156 mean deposited energy measured by the MINIPix TIMEPIX detector and simulated in GATE/Geant4 to the  
157 deposited energy calculated based on PSTAR data of proton stopping power in silicon [26].

## 158 2.5 Dose profile characterization

159 The experimental setup was used for two types of dose profile measurements. We performed lateral dose  
160 profile measurements in air to demonstrate the capability of the MINIPix TIMEPIX detector to be used for  
161 commissioning and characterization of proton therapeutic pencil beams. Next, we performed lateral and  
162 longitudinal dose profile measurements in water to validate the pencil beam propagation performed by TPS  
163 and MC simulations.

### 164 Experimental setup, beam conditions, and data acquisition

165 The MINIPix TIMEPIX detector was positioned in a dedicated, waterproof, in-house designed PMMA  
166 holder mounted inside the water phantom (BluePhantom<sup>2</sup> by IBA). We enclose the technical sketch of the  
167 PMMA holder in supplementary materials. The detector sensitive volume was positioned at isocentre using  
168 water phantom step motors and laser patient positioning system. The MINIPix TIMEPIX was positioned at  
169 an angle  $\beta = 45^\circ$ . See figure 2 middle panel for the detector placed in the phantom (in air) without the  
170 waterproof cover and figure 2 right panel for detector placed in water.

171 The lateral proton pencil beam profiles in air and in water were acquired for proton beams at nominal  
172 energies E100, E150, E200, with and without range shifter. All the measurements were performed using the  
173 lowest possible accelerator beam current of 1 nA to keep the beam current stable between measurements.  
174 For the 1 nA beam current we did not perform measurements with the detector placed in the beam core  
175 (0-20 mm away from the isocentre) because at such current the primary proton yield leads to detector  
176 saturation for a single acquisition time frame. For dose profile measurements, the time frame duration  
177 was set by the software operator based on a real-time visual assessment of the data in the PIXET PRO  
178 software. Before starting the data acquisition, while beam was on, the most optimal time frame duration  
179 was selected allowing acquisition of the maximal possible number of clusters in one frame and avoiding  
180 cluster overlapping effect. The total acquisition time of each measurement in single point of radiation field  
181 depends on particle fluence, and it was from 20 to 40 s resulting in the order of  $10^4$ - $10^6$  registered single  
182 particle events (clusters). In total, we performed 26 proton pencil beam lateral and longitudinal dose profile  
183 measurements.

184 For measurements in air, MINIPix TIMEPIX was positioned at the gantry room isocentre, and lateral  
185 profiles were acquired at the distance from 30 to 180 mm away from the isocentre. Following the  
186 measurements in air, BluePhantom<sup>2</sup> was filled with water. See figure 3 for simulated 2D dose distributions  
187 of proton pencil beams in water with and without range shifter for three investigated nominal proton beam  
188 energies. The dose distributions are overlapped with lines indicating which lateral and longitudinal dose  
189 profiles were measured. We measured lateral dose profiles at three depths, at 1/2 and 3/4 of the proton  
190 beam range, as well as in the Bragg peak position. For 150 MeV proton beam, the longitudinal profiles  
191 were measured at the distance of 25, 37, 49, and 61 mm away from the isocentre.

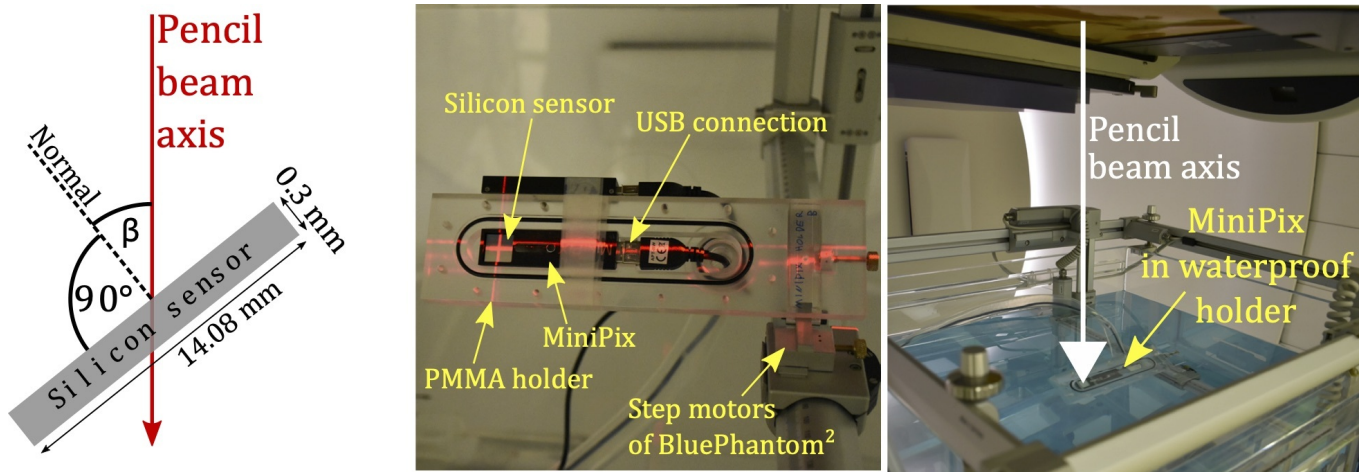


**Figure 2.** Schematic illustration of MINIPIX TIMEPIX detector silicon sensor and the definition of  $\beta$  angle between the normal to the silicon sensor surface and proton pencil beam axis (left panel), MINIPIX TIMEPIX placed in the PMMA holder positioned in water phantom without the waterproof cover (middle panel), and immersed in the water phantom filled with water for profile measurements (right panel).

## 192 Monte Carlo simulations

193 The dose distributions in water for the nominal energies used in the experiment with and without the  
 194 RS were calculated using clinical TPS (analytical dose computation algorithm), as well as simulated in  
 195 GATE/Geant4 and FRED MC engines. In GATE/Geant4, we used the QGSP\_BIC\_HP\_EMZ physics list with  
 196 1 mm production cut for gammas, electrons, and positrons and  $10\ \mu\text{m}$  for protons. In both MC engines, a  
 197 high statistics of  $10^9$  primaries were simulated in order to obtain the beam dose envelope in water up to  
 198 150 mm far from the beam core. The dose was scored in water in  $2 \times 2 \times 2\ \text{mm}^3$  voxels.

## 199 2.6 Data analysis

200 The data pre-processing was performed using PIXET PRO track processing tool, which provided a list of  
 201 clusters and their parameters for each measurement performed at the given point of radiation field. For  
 202 analysis of the dose profiles we extracted from PIXET PRO: (i) the total energy deposition in each cluster,  
 203 (ii) the cluster position in the detector sensor as well as (iii) the total number of frames and (iv) the frame  
 204 duration time for each measurement point. For each measurement point we calculated the relative dose rate  
 205 D as:

$$D = \frac{1}{t_{\text{acq}} \cdot n} \cdot \frac{\sum_i E_i}{m} \quad [\text{Gy/s}], \quad (1)$$

206 where  $E_i$  is the total energy deposited by a particle in a cluster,  $m$  is the mass of the detector silicon sensor,  
 207  $t_{\text{acq}}$  is the frame acquisition time (constant within one measurement point), and  $n$  is the total number of  
 208 frames acquired in one measurement point.

209 The visualization and comparison of the lateral dose profiles obtained experimentally in air and in water  
 210 to simulations was performed as follows. The maximum value of the lateral beam dose profile simulated  
 211 in GATE/Geant4, FRED, and TPS were normalized. The dose experimental profiles were adjusted to the  
 212 corresponding simulated profiles using least mean square algorithm. This was necessary because the dose  
 213 rate at the profile maximum varies depending on primary beam energy and on measurement depth. The  
 214 value of relative dose rate obtained experimentally was not modified between the measurement points  
 215 within a single profile.

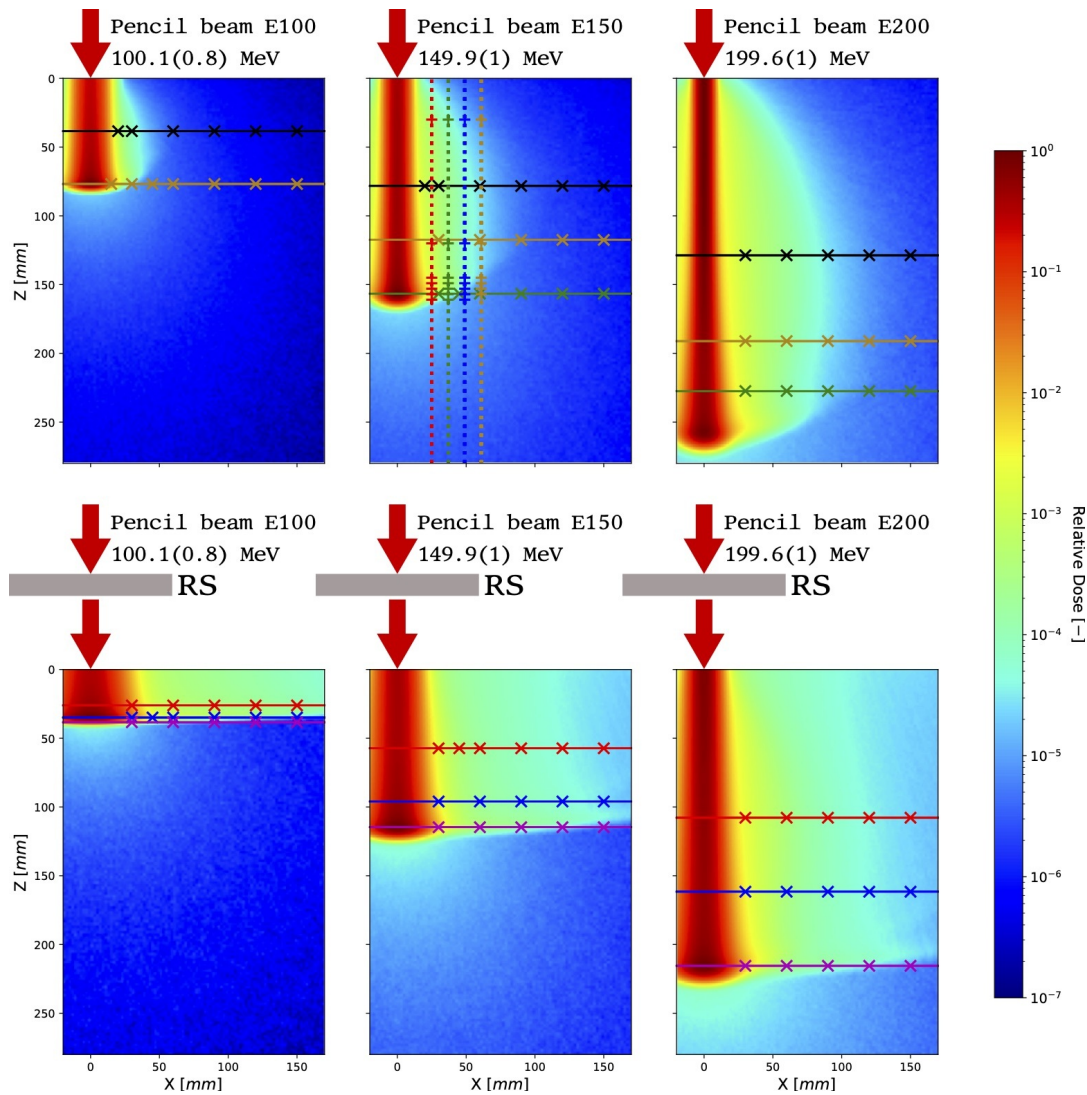


**Figure 3.** 2D dose profiles obtained from MC simulation of proton beams at three nominal energies with (bottom) and without (top) the RS. The lateral and longitudinal dose profiles measured with MINIPix TIMEPIX are shown, and the measurement points are marked with crosses. The color convention used to illustrate measured dose profiles is the same as the one used in the figures in the results sections 3.3 and 3.4.

216 Next, we compared lateral and longitudinal dose profiles measured with MINIPix TIMEPIX in water  
 217 with the simulations of 3D dose profiles performed with clinical TPS, fast MC code FRED, and full MC  
 218 code GATE/Geant4. A median filter with kernel size of 5 was used for lateral GATE/Geant4 profiles at  
 219 the distance larger than 50 mm from the beam core to compensate for the statistical fluctuations of MC  
 220 simulation.

221 For the purpose of visualization of the longitudinal dose profile measurement in water, the maximum  
 222 value of the 3D dose distribution simulated in GATE/Geant4, FRED, and TPS was normalized to 1. The  
 223 longitudinal profiles simulated at the distance from beam core are plotted according to the normalization,  
 224 and the MINIPix TIMEPIX measurement results were adjusted to the simulations using the same least  
 225 mean square algorithm.

### 3 RESULTS

#### 3.1 Calibration measurements

Figure 4 (left panel) shows an example of energy deposition spectra for detector angle  $\beta=57^\circ$  (cf. figure 2 left panel) and nominal proton energy E150. The spectrum obtained experimentally (raw data) exhibits considerable amount of clusters with low energy depositions (below 0.4 MeV) and particles incoming at significantly smaller angles than  $\beta$ . These clusters are produced mostly by photons originating from the gantry nozzle equipment (plane-parallel and multiwire ionisation chambers), which are not explicitly simulated in the GATE/Geant4. The main energy deposition peak, with the maximum of about 0.5 MeV, is produced by the protons entering the detector at angle  $57\pm 3^\circ$ . The peaks to the right, with the maximum of about 1 MeV and 1.6 MeV, result from the overlapping effect, where respectively two or three primary protons overlap creating a single clusters with the doubled or tripled energy deposition. The overlapped clusters exhibit larger incident angles than the primaries in the main energy deposition peak. The overlapping effect is not taken into account in GATE/Geant4 simulations. In order to compare the spectra obtained experimentally with the MC simulations, all the particles incoming at angles different than  $57\pm 3^\circ$  were filtered out. Figure 4 (left panel) shows the spectra obtained experimentally before and after filtering, spectra obtained from simulations, and measured angle of the incoming particles as a function of deposited energy.

Figure 4 (middle panel) shows energy deposition spectra for nominal energy E150 and various  $\beta$  angles. The main energy deposition peak shapes and positions are comparable with the simulations. The mean deposited energy obtained from MINIPIX TIMEPIX measurements (after filtering), simulated in GATE/Geant4 MC and calculated based on PSTAR stopping power data are presented in figure 4 (right panel). The best agreement is achieved for detector angles  $\beta$  up to  $73^\circ$ . For angles higher than  $73^\circ$ , the mean energy deposition obtained from simulations is consistent with the PSTAR data but it is higher for measurements. This might be an effect of registering particles scattered on the MINIPIX TIMEPIX case made of aluminum, which produce long clusters of large energy depositions. Therefore, for the beam profile measurements in water and in air, the detector angles of  $45^\circ$  or  $60^\circ$  were chosen.

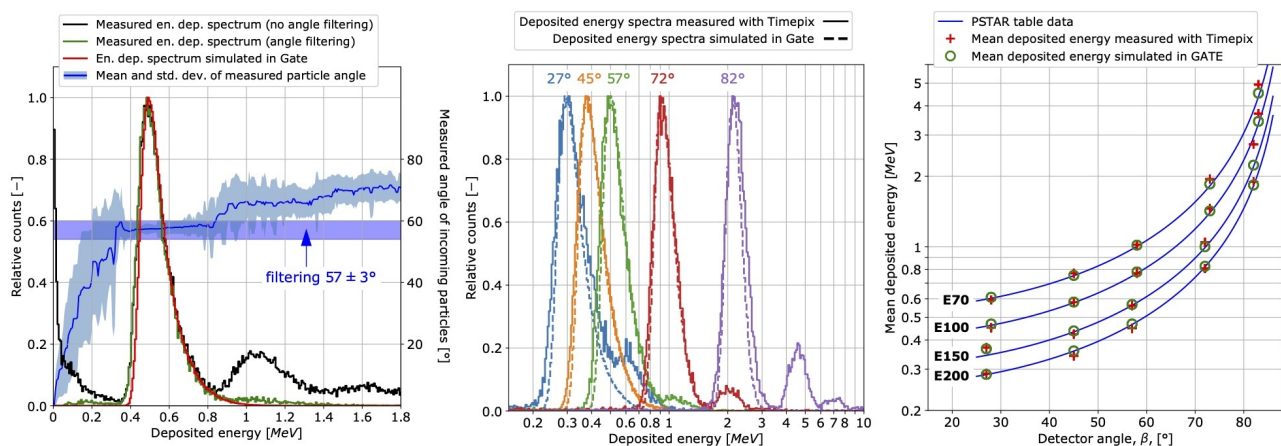


**Figure 4.** Example of energy deposition spectrum for proton beam at the nominal energy E150 measured with MINIPIX TIMEPIX positioned at angle  $\beta=57^\circ$  before and after filtering for the particles incidence angle ( $\pm 3^\circ$ ) as well as the one obtained from GATE/Geant4 MC simulation (left panel). Energy deposition spectra after applying the cluster filtering procedure for nominal energy E150 and various  $\beta$  detector angles (middle panel). Mean energy deposited in MINIPIX TIMEPIX exposed to nominal proton energies E70, E100, E150, and E200 when positioned at various angles. The measurement results are compared to MC simulations and data calculated based on PSTAR stopping power tables (right panel).

### 251 3.2 Beam spot profiles in air

252 Figure 5 shows proton pencil beam lateral profiles measured for nominal energies E100, E150, and E200  
 253 in air, at the isocentre, without and with the RS. The profile shapes measured with MINIPix TIMEPIX  
 254 correspond well to TPS beam model data obtained during the facility commissioning. The high sensitivity  
 255 of MINIPix TIMEPIX allowed to perform measurements in significant distance from the beam core (from  
 256 30 mm up to 180 mm) in relative dose range of 3 orders of magnitude. This allowed to measure the build  
 257 up of the nuclear halo.

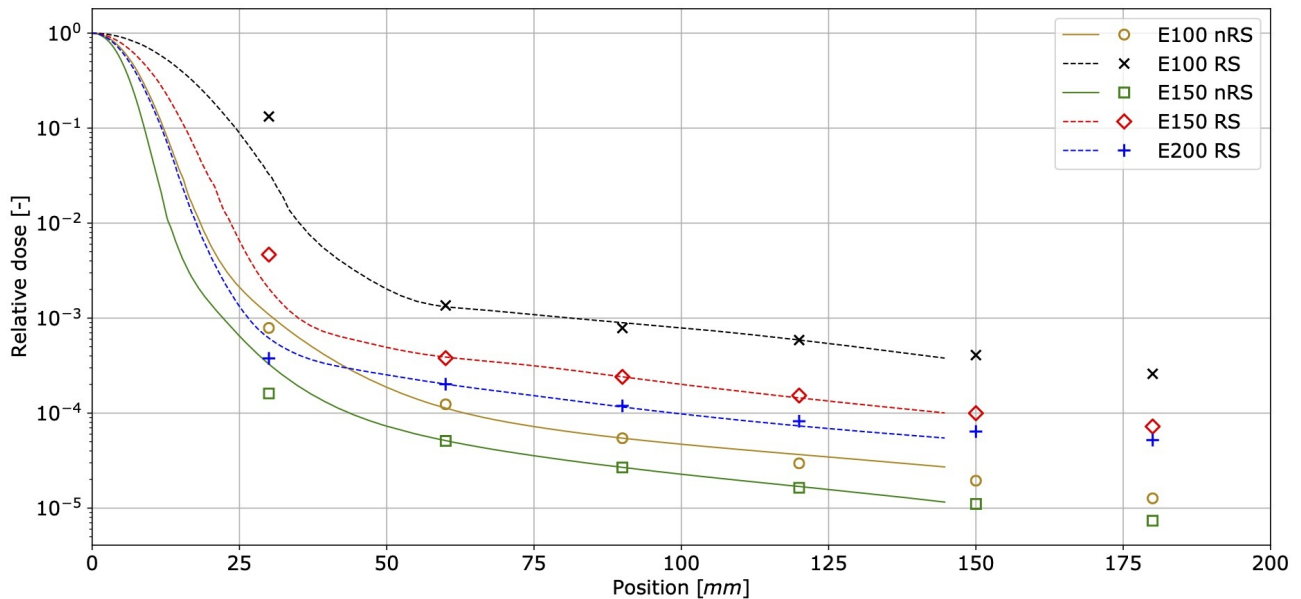


**Figure 5.** Lateral pencil beam dose profiles measured at the gantry room isocentre in air for primary proton beams at three nominal energies. Points correspond to MINIPix TIMEPIX measurement results, whereas solid and dashed lines are the data obtained from TPS beam model without RS (nRS) and with RS, respectively.

### 258 3.3 Lateral profiles in water

259 Figure 6 shows MINIPix TIMEPIX results in water performed with and without the RS for three nominal  
 260 beam energies E100, E150, and E200. The measurement results of (i) the first Gaussian term obtained  
 261 with the LYNX scintillating screen and (ii) the low-dose envelope (nuclear halo) obtained with MINIPix  
 262 TIMEPIX are compared with GATE/Geant4 and FRED MC simulations.

263 We observed an excellent agreement between the shape of the profiles obtained experimentally with  
 264 LYNX and MINIPix TIMEPIX and simulated with full MC code GATE/Geant4 up to 150 mm far from  
 265 the beam core. The shape of the lateral dose profiles were also accurately reproduced at different depths  
 266 in water and behind the RS. In FRED simulations, the shape of the lateral dose profiles in comparison to  
 267 MINIPix TIMEPIX measurements is well mimicked up to 4 orders of magnitude. The disagreement for  
 268 more distant measurement points is due to the fact the FRED code does not transport secondary gammas  
 269 and electrons.

### 270 3.4 Longitudinal profiles in water

271 Figure 7 presents proton pencil beam longitudinal dose profiles in water for beam nominal energy E150.  
 272 The beam range measured with MINIPix TIMEPIX is in agreement with the GATE/Geant4 simulations,  
 273 even at the distance of 61 mm from the beam core, whereas TPS does not predict any dose at this distance.

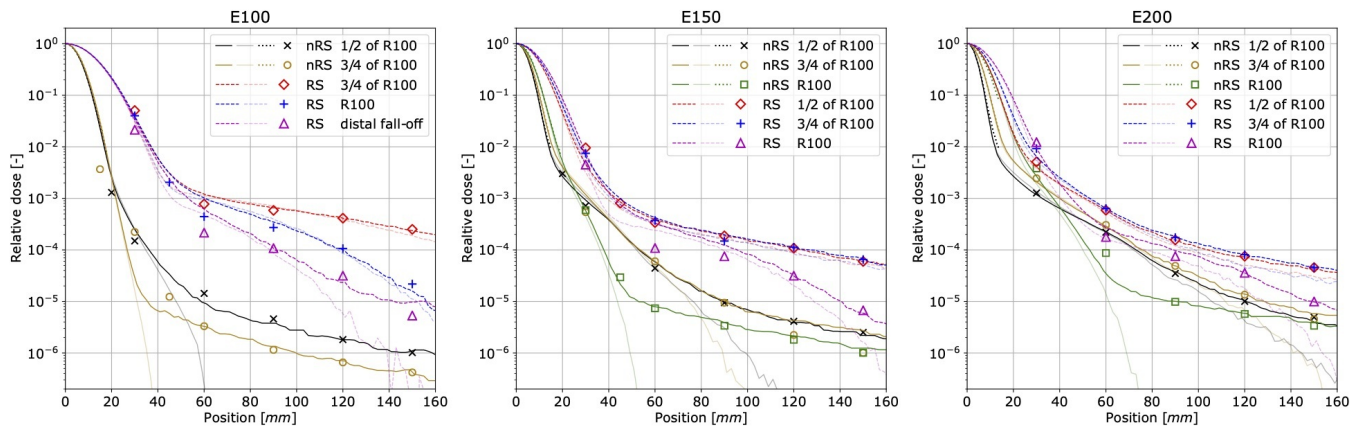


**Figure 6.** Lateral beam dose profiles measured in water at different depths for three beam nominal energies. Points correspond to MINIPIX TIMEPIX measurement results, dotted lines are results of measured with LYNX detector, whereas solid and dashed lines are the GATE/Geant4 data without (nRS) and with RS, respectively. Corresponding transparent lines presents FRED simulations result.

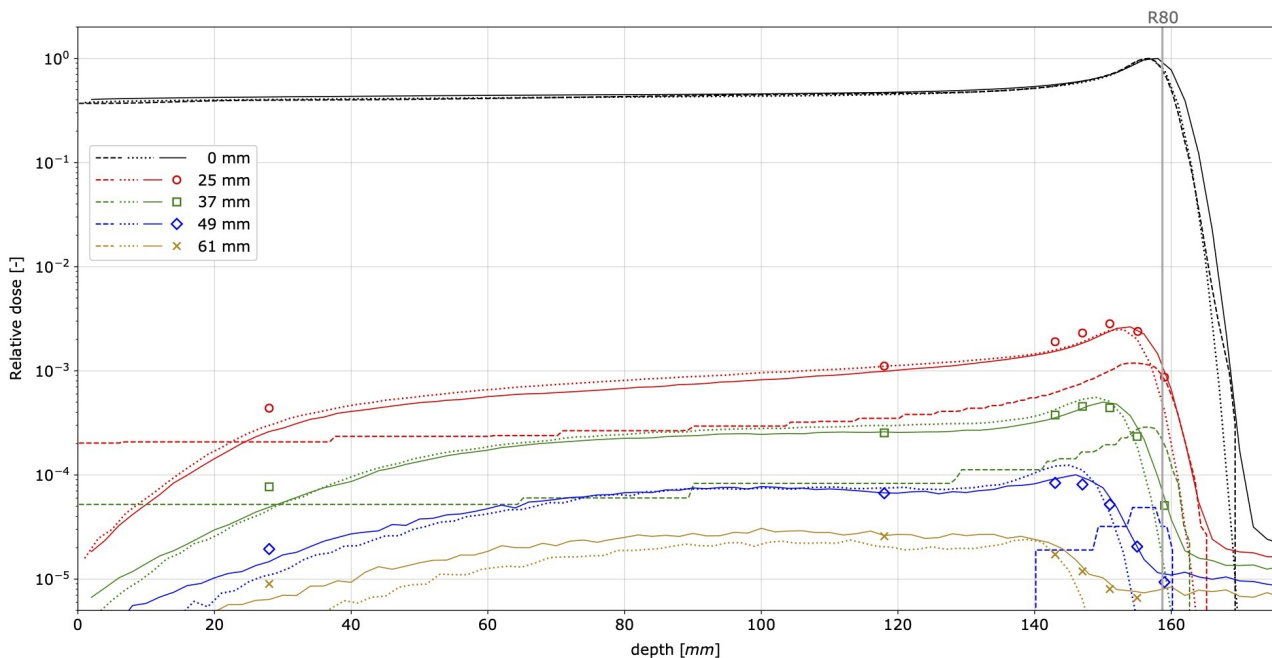


**Figure 7.** Longitudinal pencil beam dose profiles measured in water for proton beam nominal energy E150. Points correspond to MINIPIX TIMEPIX measurement results, whereas solid, dotted, and dashed lines to GATE/Geant4, FRED, and TPS simulations, respectively. The mean proton range of 158.7 mm is marked by a vertical line (R80).

### 4 DISCUSSION

274 In the frame of this work we performed a validation of the detector calibration for protons, and the  
 275 measurements of the beam dose profiles in air and in water. The comparison of the calibration measurements  
 276 and MC simulations demonstrate that the MINIPIX TIMEPIX accurately measures energy deposited by  
 277 proton beams. The comparison of the mean energy deposition in the detector to MC simulation results  
 278 and PSTAR data indicates that positioning of the detector at 45° with respect to the beam axis is the most  
 279 optimal for the measurements. Here we performed only the validation of the calibration for protons in  
 280 energy range from 70 to 200 MeV, whereas in the mixed radiation field in water, a wider energy spectrum

281 of particles can be registered by the detector. The response of the MINIPix TIMEPIX detector to other  
282 radiation types was studied elsewhere [27].

283 The measurements of the lateral and longitudinal pencil beam dose profiles performed with the MINIPix  
284 TIMEPIX detector show its capability to measure the dose with the dynamic range of up to 4 orders of  
285 magnitude. The measurements of the beam lateral profiles in air correspond well to the TPS beam model  
286 data obtained during the facility commissioning. The beam lateral and longitudinal profiles measured in  
287 water are in an excellent agreement with GATE/Geant4 simulations. Because of the limited time resolution  
288 of the MINIPix TIMEPIX detector, it was not possible to perform measurements in the beam core, where  
289 the fluence of particles was high, causing detector saturation. A new generation of the TIMEPIX detectors,  
290 the MINIPix TIMEPIX 3 (ADVACAM), offers time resolution better than the MINIPix TIMEPIX used in  
291 this work. MINIPix TIMEPIX 3 will allow for measurements in the beam core and in therapeutic fields,  
292 where the particle fluence is high. In order to minimize the fraction of particles scattered on the aluminum  
293 detector case, an alternative, e.g., PMMA case, should be considered.

294 Since MINIPix TIMEPIX provides information about a single particle energy deposition and its track  
295 length, it is possible to calculate the linear energy transfer (LET) value of each particle penetrating the  
296 detector sensor. Future work will focus on an experimental characterization of the energy deposition and  
297 the LET spectra in mixed radiation fields produced by therapeutic proton beams in water. The results will  
298 be used for validation of MC codes and TPS, aiming at improved physical and biological modeling in  
299 proton radiotherapy.

## CONFLICT OF INTEREST STATEMENT

300 The authors declare that the research was conducted in the absence of any commercial or financial  
301 relationships that could be construed as a potential conflict of interest.

## AUTHOR CONTRIBUTIONS

302 PS, AR, JG, CG, GK, CO, MPN, SN, MR performed the experiments. PS and JG made the experiment  
303 data analysis and prepared figures. CG and CO provided expertise in MINIPix TIMEPIX data analysis. JG  
304 performed the MC simulations, analyzed the data and prepared figures. MPN and JB provided expertise  
305 in GATE/Geant4 MC simulations and data analysis. AS developed and made substantial improvements  
306 in FRED source code required to enable presented studies. PS, AR, and JG drafted the manuscript. NK  
307 extensively reviewed the manuscript. AR and JG designed the project and AR acquired funding.

## FUNDING

308 This project is carried out within the Reintegration programme of the Foundation for Polish Science  
309 co-financed by the EU under the European Regional Development Fund – grant no. POIR.04.04.00-00-  
310 2475/16-00.

## ACKNOWLEDGMENTS

311 We acknowledge Aleksander Krempa from Krakow proton therapy center for IT support during  
312 implementation of this project. This research was supported in part by computing resources of ACC  
313 Cyfronet AGH. We acknowledge the support of NVIDIA Corporation with the donation of the GPU used  
314 for FRED MC simulations.

## REFERENCES

- 315 [1] Durante M, Orecchia R, Loeffler JS. Charged-particle therapy in cancer: clinical uses and future  
316 perspectives. *Nat. Rev. Clin. Oncol.* **14** (2017) 483.
- 317 [2] Durante M. Proton beam therapy in Europe: more centres need more research. *British Journal of*  
318 *Cancer* (2018) 777–778. doi:10.1038/s41416-018-0329-x.
- 319 [3] Harms J, Chang CW, Zhang R, Lin L. Nuclear halo measurements for accurate prediction of field  
320 size factor in a Varian ProBeam proton PBS system. *Journal of Applied Clinical Medical Physics* **21**  
321 (2020) 197–204. doi:10.1002/acm2.12783.
- 322 [4] Zhu RX, Poenisch F, Lii M, Sawakuchi GO, Titt U, Bues M, et al. Commissioning dose computation  
323 models for spot scanning proton beams in water for a commercially available treatment planning  
324 system. *Medical Physics* **40** (2013) 041723. doi:10.1118/1.4798229.
- 325 [5] Gajewski J, Kłosowski M, Olko P. Two-Dimensional Thermoluminescence Dosimetry System for  
326 Proton Beam Quality Assurance. *Radiation Measurements* **90** (2016) 224–227. doi:http://dx.doi.org/  
327 10.1016/j.radmeas.2015.12.019.
- 328 [6] Sądel M, Bilski P, Sankowska M, Gajewski J, Swakoń J, Horwacik T, et al. Two-dimensional  
329 radiation dosimetry based on LiMgPO<sub>4</sub> powder embedded into silicone elastomer matrix. *Radiation*  
330 *Measurements* **133** (2020). doi:10.1016/j.radmeas.2020.106255.
- 331 [7] Rydygier M, Jastrzab M, Krzempek D, Nowak T, Grzanka L, Bednarczyk P, et al. Radiotherapy  
332 proton beam profilometry with scCVD diamond detector in single particle mode. *Radiation Protection*  
333 *Dosimetry* **180** (2018) 282–285. doi:10.1093/RPD/NCX305.
- 334 [8] Karger CP, Jäke O, Palmans H, Kanai T. Dosimetry for ion beam radiotherapy. *Phys Med Biol* **55**  
335 (2010) R193–R234.
- 336 [9] Schiavi A, Senzacqua M, Pioli S, Mairani A, Magro G, Molinelli S, et al. Fred: a GPU-accelerated  
337 fast-Monte Carlo code for rapid treatment plan recalculation in ion beam therapy. *Physics in Medicine*  
338 *and Biology* **62** (2017) 7482–7504. doi:10.1088/1361-6560/aa8134.
- 339 [10] Gajewski J, Garbacz M, Chang CW, Czerska K, Durante M, Krah N, et al. Commissioning  
340 of GPU-accelerated Monte Carlo code Fred for clinical applications in proton therapy.  
341 [https://www.ifj.edu.pl/oddzialy/no6/nz62/ar/wp-content/uploads/2020/02/Fred2020\\_submitted.pdf](https://www.ifj.edu.pl/oddzialy/no6/nz62/ar/wp-content/uploads/2020/02/Fred2020_submitted.pdf).  
342 *Frontiers in Physics - Medical Physics and Imaging* (2020) submitted to this issue.
- 343 [11] Martíková M, Jakubek J, Granja C, Hartmann B, Oplka L, Pospíšil S, et al. Measurement of secondary  
344 radiation during ion beam therapy with the pixel detector Timepix. *Journal of Instrumentation* **6**  
345 (2011). doi:10.1088/1748-0221/6/11/C11014.
- 346 [12] Opalka L, Granja C, Hartmann B, Jakubek J, Jaekel O, Martisikova M, et al. Linear energy transfer  
347 and track pattern recognition of secondary radiation generated in hadron therapy beam in a PMMA  
348 target. *Journal of Instrumentation* **8** (2013). doi:10.1088/1748-0221/8/02/C02047.
- 349 [13] Rosenfeld AB. Electronic dosimetry in radiation therapy. *Radiation Measurements* **41** (2006) 134–153.  
350 doi:10.1016/j.radmeas.2007.01.005.
- 351 [14] Reza S, Wong WS, Fröjd E, Norlin B, Fröjd C, Thungström G, et al. Smart dosimetry by pattern  
352 recognition using a single photon counting detector system in time over threshold mode. *Journal of*  
353 *Instrumentation* **7** (2012). doi:10.1088/1748-0221/7/01/C01027.
- 354 [15] Rubovič P, Bergmann B, Ekendahl D, Hůlka J, Judas L, Kohout Z, et al. Timepix detector as a tool for  
355 X-ray and gamma dosimetry. *Radiation Measurements* **107** (2017) 39–42. doi:10.1016/j.radmeas.  
356 2017.10.012.
- 357 [16] George SP, Severino CT, Fröjd E, Murtas F, Silari M. Measurement of an accelerator based mixed field  
358 with a Timepix detector. *Journal of Instrumentation* **10** (2015). doi:10.1088/1748-0221/10/03/P03005.

- 359 [17] Kroupa M, Bahadori A, Campbell-Ricketts T, Empl A, Hoang SM, Idarraga-Munoz J, et al. A  
360 semiconductor radiation imaging pixel detector for space radiation dosimetry. *Life Sciences in Space*  
361 *Research* **6** (2015) 69–78. doi:10.1016/j.lssr.2015.06.006.
- 362 [18] Stoffle N, Pinsky L, Kroupa M, Hoang S, Idarraga J, Amberboy C, et al. Timepix-based radiation  
363 environment monitor measurements aboard the International Space Station. *Nuclear Instruments*  
364 *and Methods in Physics Research, Section A: Accelerators, Spectrometers, Detectors and Associated*  
365 *Equipment* **782** (2015) 143–148. doi:10.1016/j.nima.2015.02.016.
- 366 [19] Turecek D, Pinsky L, Jakubek J, Vykydal Z, Stoffle N, Pospisil S. Small Dosimeter based on Timepix  
367 device for International Space Station. *Journal of Instrumentation* **6** (2011). doi:10.1088/1748-0221/  
368 6/12/C12037.
- 369 [20] Ballabriga R, Campbell M, Llopart X. Asic developments for radiation imaging applications: The  
370 medipix and timepix family. *Nuclear Instruments and Methods in Physics Research, Section A:*  
371 *Accelerators, Spectrometers, Detectors and Associated Equipment* **878** (2018) 10–23. doi:10.1016/j.  
372 nima.2017.07.029.
- 373 [21] Granja C, Jakubek J, Polansky S, Zach V, Krist P, Chvatil D, et al. Resolving power of pixel detector  
374 Timepix for wide-range electron, proton and ion detection. *Nuclear Instruments and Methods in*  
375 *Physics Research, Section A: Accelerators, Spectrometers, Detectors and Associated Equipment* **908**  
376 (2018) 60–71. doi:10.1016/j.nima.2018.08.014.
- 377 [22] Granja C, Kudela K, Jakubek J, Krist P, Chvatil D, Stursa J, et al. Directional detection of charged  
378 particles and cosmic rays with the miniaturized radiation camera MiniPIX Timepix. *Nuclear*  
379 *Instruments and Methods in Physics Research, Section A: Accelerators, Spectrometers, Detectors and*  
380 *Associated Equipment* **911** (2018) 142–152. doi:10.1016/j.nima.2018.09.140.
- 381 [23] Sarrut D, Bardiès M, Bousson N, Freud N, Jan S, Létang J, et al. A review of the use and potential of  
382 the GATE Monte Carlo simulation code for radiation therapy and dosimetry applications. *Medical*  
383 *Physics* **41** (2014) 64301. doi:10.1118/1.4871617.
- 384 [24] Jakubek J, Granja C, Hartmann B, Jaekel O, Martisikova M, Opalka L, et al. Selective detection  
385 of secondary particles and neutrons produced in ion beam therapy with 3D sensitive voxel detector.  
386 *Journal of Instrumentation* **6** (2011). doi:10.1088/1748-0221/6/12/C12010.
- 387 [25] Kroupa M, Campbell-Ricketts T, Bahadori A, Empl A. Techniques for precise energy calibration of  
388 particle pixel detectors. *Review of Scientific Instruments* **88** (2017). doi:10.1063/1.4978281.
- 389 [26] [Dataset] Berger MJ, Coursey JS, Zucker MA, Chang J. Stopping-Power & Range Tables for Electrons,  
390 Protons, and Helium Ions (2017).
- 391 [27] Granja C, Oancea C, Jakubek J, Benton E, Kodaira S, Rucinski A, et al. Wide-  
392 Range Tracking and LET-Spectra of Energetic Light and Heavy Charged Particles.  
393 <https://www.ifj.edu.pl/oddzialy/no6/nz62/ar/wp-content/uploads/2020/05/Granja2020.pdf>. *submitted*  
394 *to Nuclear Instruments and Methods in Physics Research A* (2020).